DOI: 10.1111/exd.12932
www.wileyonlinelibrary.com/journal/EXD

Original Article

Longitudinal *in vivo* tracking of adverse effects following topical steroid treatment

Andrew J. Bower[1,2], Zane Arp[3], Youbo Zhao[1], Joanne Li[4], Eric J. Chaney[1], Marina Marjanovic[1,4], Angela Hughes-Earle[3] and Stephen A. Boppart[1,2,4,5]

[1]Beckman Institute for Advanced Science and Technology, University of Illinois at Urbana-Champaign, Urbana, IL, USA; [2]Department of Electrical and Computer Engineering, University of Illinois at Urbana-Champaign, Urbana, IL, USA; [3]GlaxoSmithKline, King of Prussia, PA, USA; [4]Department of Bioengineering, University of Illinois at Urbana-Champaign, Urbana, IL, USA; [5]Department of Internal Medicine, University of Illinois at Urbana-Champaign, Urbana, IL, USA

Correspondence: Stephen A. Boppart, Beckman Institute for Advanced Science and Technology, University of Illinois at Urbana-Champaign, 405 N. Mathews Avenue, Urbana, IL, 61801 USA, Tel: 217-244-7479 , Fax: 217-333-5833, email: boppart@illinois.edu

Abstract: Topical steroids are known for their anti-inflammatory properties and are commonly prescribed to treat many adverse skin conditions such as eczema and psoriasis. While these treatments are known to be effective, adverse effects including skin atrophy are common. In this study, the progression of these effects is investigated in an *in vivo* mouse model using multimodal optical microscopy. Utilizing a system capable of performing two-photon excitation fluorescence microscopy (TPEF) of reduced nicotinamide adenine dinucleotide (NADH) to visualize the epidermal cell layers and second harmonic generation (SHG) microscopy to identify collagen in the dermis, these processes can be studied at the cellular level. Fluorescence lifetime imaging microscopy (FLIM) is also utilized to image intracellular NADH levels to obtain molecular information regarding metabolic activity following steroid treatment. In this study, fluticasone propionate (FP)-treated, mometasone furoate (MF)-treated and untreated animals were imaged longitudinally using a custom-built multimodal optical microscope. Prolonged steroid treatment over the course of 21 days is shown to result in a significant increase in mean fluorescence lifetime of NADH, suggesting a faster rate of maturation of epidermal keratinocytes. Alterations to collagen organization and the structural microenvironment are also observed. These results give insight into the structural and biochemical processes of skin atrophy associated with prolonged steroid treatment.

Key words: fluorescence lifetime imaging microscopy – multiphoton microscopy – second harmonic generation microscopy – skin atrophy – topical steroids

Accepted for publication 21 December 2015

Introduction

Glucocorticoids remain the most broadly used anti-inflammatory drugs in clinical practice (1). Since the introduction of topical hydrocortisone in the early 1950s, these drugs have been used for localized treatment of inflammatory skin disorders such as eczema and psoriasis (2). However, there are many adverse side effects caused by topical steroid treatment, often associated with skin atrophy. Skin atrophy is characterized by a loss of the barrier function which can result in increased permeability and transepidermal water loss (3). In addition, the atrophied area is much more fragile and has greater potential for tearing, bruising and infection. In treatment regimens utilizing superpotent steroids, these effects can be quite severe and are potentially irreversible (1).

Histological analysis of topical skin steroid treatment in humans and in animal models has found a decrease in the number of keratinocytes and fibroblasts (4), a decrease in the size of keratinocytes (5), reduced epidermal thickness (6) and a relatively flat dermal–epidermal junction (7) compared to untreated skin. Topical steroids have also been shown to decrease the proliferation rates of keratinocytes and fibroblasts (8,9) as well as accelerate the maturation of these cells (10). A decrease in type I collagen production by dermal fibroblasts has also been observed (11). This results in a reorganization of the collagen fibres in which dense, compact bundles are formed in place of the more structurally sound 'basket weave' meshwork (12). Even with these observations, the exact mechanism responsible for the adverse effects due to topical steroid treatment remains elusive (13).

Current methods that exist for assessing the skin atrophy potential *in vivo* in humans or animal models include X-ray (14) and ultrasound (4) measurements of skin thickness, as well as dermoscopic observation of the skin surface (15). For X-ray and ultrasound measurements, only structural thickness changes may be observed with low resolution, and the progression of functional changes such as cellular metabolism cannot be measured. Dermoscopic observations provide only magnified photographs of the skin surface, ignoring the important depth-dependent information needed to assess early changes associated with skin atrophy. New optical microscopy methods for the evaluation of the atrophogenic potential of topical corticosteroids have been developed to enable non-invasive probing of the structural and functional properties of the skin microenvironment in an effort to better understand, observe and track adverse reactions to topical steroid treatment in skin. Laser scanning confocal microscopy (LSCM) has allowed the visualization of keratinocytes *in vivo*, allowing changes in cell size to be observed in human patients (4). More recently, multiphoton microscopy (MPM) has been used to distinguish keratinocytes and collagen in the skin, allowing both visualization of the skin

cell layers and measurements of skin thickness (16). However, in these studies, only structural information about the skin thickness and cell layers was obtained and any molecular or functional changes were largely ignored.

In this study, functional parameters regarding epidermal cell metabolism and structural measures of dermal collagen in the corticosteroid-treated skin microenvironment are measured simultaneously using a multimodal optical microscope. While in previous studies, the focus was mainly on identifying structural changes within epidermal keratinocytes (4,16), the focus here is instead to study the metabolic environment of epidermal keratinocytes which may precede epidermal thinning. With this imaging system, subtle changes resulting from steroid treatment are observed that cannot otherwise be detected with LSCM or MPM alone. This multimodal microscope allows for the simultaneous acquisition of images utilizing two-photon excited fluorescence (TPEF), second harmonic generation (SHG) and fluorescence lifetime imaging microscopy (FLIM). TPEF is a nonlinear fluorescence imaging technique in which exogenous or endogenous fluorophores are excited with the simultaneous absorption of two photons (17). SHG is a nonlinear imaging technique highly sensitive to non-centrosymmetric crystalline structure (18). FLIM is an additive detection scheme to TPEF imaging in which the lifetime of the fluorescence emitted from the fluorophores is measured, allowing sensitive quantification of metabolism (19), pH (20), local oxygen and calcium concentrations (21,22), as well as other important biological parameters. Previously, this multimodal microscope has been used to assess and quantify wound healing parameters (23,24), to investigate cell death processes (25) and to evaluate human engineered skin constructs (26). In this study, TPEF and FLIM are used to follow the structural and metabolic changes of keratinocytes and SHG is used to identify alterations in the organization and structure of collagen networks following treatment with fluticasone propionate (FP) (27) and mometasone furoate (MF) (28). For the steroids used in this study, FP is a class 5 topical steroid and MF, which is slightly more potent, is listed as a class 4 topical steroid.

Methods

Study design

In this study, a hairless mouse model (SKH1-Elite, Charles River) was used to investigate the longitudinal structural and functional alterations in the skin microenvironment. This model has been used previously to study the effects of topical steroid-induced atrophy (29). Fifteen mice were separated into three groups of five mice each. One group was untreated while the other two groups were treated with either FP (0.05% cream, Fougera, class 5 topical steroid) or MF (0.1% cream, Merck Elocon, class 4 topical steroid). Steroid-treated animals were imaged on days 1, 3, 7, 14 and 21. The untreated control group was imaged on days 1, 7, 14 and 21. After each imaging session, one animal was removed from the study and a skin sample was excised from the area of the imaging site for direct histological comparison of longitudinal changes. All studies were conducted under a protocol approved by the University of Illinois at Urbana-Champaign Institutional Animal Care and Use Committee (IACUC) and the GlaxoSmithKline Policy on the Care, Welfare and Treatment of Laboratory Animals.

Integrated multimodal optical microscope

A custom-built multimodal optical microscope was used to perform the imaging (Figure S1). The unique combination of TPEF, SHG and FLIM can provide both structural and functional information regarding the skin microenvironment with cellular resolution. Excitation light was provided by a titanium:sapphire laser (MaiTai HP, Spectra Physics, Santa Clara, CA, USA) centred at a wavelength of 730 nm, which was focused beneath the skin using a high numerical aperture (NA) objective lens (XLUMP20X, Olympus, Tokyo, Japan). The optical power at the focus was less than seven milliwatts. The focal spot was raster scanned transversely across the sample using a pair of computer-controlled galvanometric mirrors (Micromax 671, Cambridge Technology, Bedford, MA, USA). Detection of fluorescence and SHG was performed using a 16 channel photomultiplier tube (PMT) spectrometer (PML-16-C, Becker & Hickl GmbH, Berlin, Germany) centred at 450 nm, allowing clear spectral separation of the collected SHG and fluorescence photons. To obtain fluorescence lifetime curves, time-correlated single photon counting (TCSPC) was performed using a commercial TCSPC data acquisition board (SPC-150, Becker & Hickl GmbH, Berlin, Germany). For FLIM imaging, data were acquired from approximately the second keratinocyte layer in the epidermis. For SHG imaging, a stack of images spanning the superficial dermis was acquired for each animal. Data analysis was performed for TPEF and SHG images using both MATLAB (MathWorks, R2014a) and ImageJ (National Institutes of Health, v. 1.47 m), while FLIM analysis was performed using SPCImage (Becker-Hickl, v. 3.0.8.0).

Statistical analysis of NADH fluorescence lifetime images

To directly compare the *in vivo* response of the three experimental groups, statistical analysis of the cellular response to the treatment at each imaging time point was performed. It is well established *in vivo* in skin that the metabolism of epidermal keratinocytes has an appreciable depth dependence (30) leading to a depth-dependent response of the mean fluorescence lifetime of NADH as well. Therefore, it is quite important to compare measurements across cellular regions from the images which contain cells of approximately the same size. However, as the skin of the mice used in these experiments is approximately 10–15 μm thick and only a few cell layers are present in the epidermis (29), it can be quite difficult to acquire data from cellular regions of approximately the same size. Therefore, to accurately compare the data across each experimental group, regions of interest containing patches of cells from approximately the second layer were manually selected for analysis. This also removes the effect of folds and artifacts clearly present in the skin as seen in Figs 1 and 2. The fluorescence lifetime values from these regions of interest were ultimately used to directly compare the effects of the different treatments to control measurements using the Student's *t*-test.

Quantification of local collagen alignment and density

Local collagen alignment was assessed quantitatively using the 2D spatial Fourier transform of local image patches or regions of interest. Collagen alignment has been assessed previously on a more global scale through the use of the 2D Fourier transform of the entire acquired SHG image (31). The orientation index, a metric for describing the relative degree of orientation, was described by finding the aspect ratio of the fitted ellipse to a binarized mask

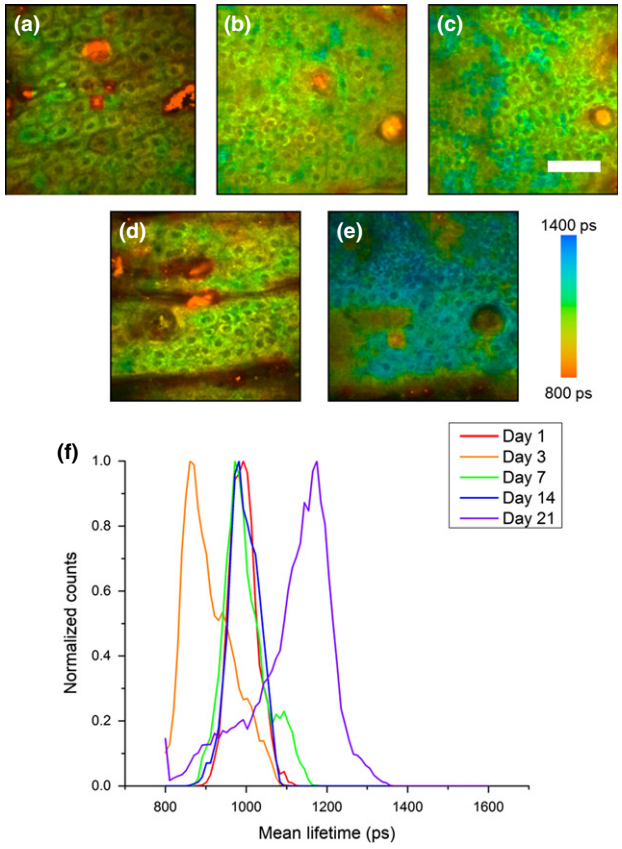

Figure 1. Longitudinal FLIM imaging of fluticasone propionate (FP)-treated animals. Lifetime imaging of keratinocytes in the epidermis at days 1 (a), 3 (b), 7 (c), 14 (d) and 21 (e) in an animal treated twice daily with FP. Normalized histograms of mean NADH lifetime of cell regions show a noticeable increase in mean lifetime at day 21 (f). Scale bar is 50 μm. ps – picoseconds.

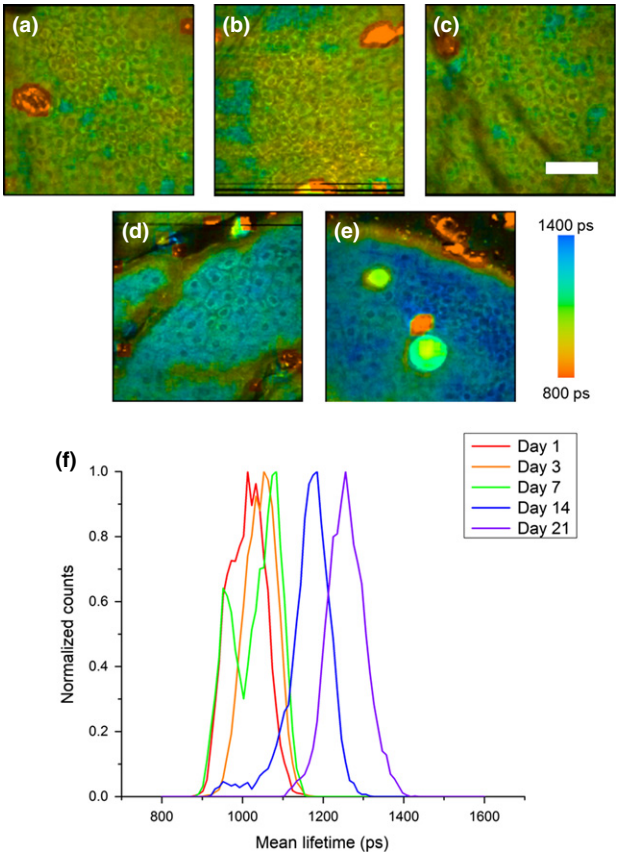

Figure 2. Longitudinal FLIM imaging of mometasone furoate (MF)-treated animals. Lifetime imaging of keratinocytes in the epidermis at days 1 (a), 3 (b), 7 (c), 14 (d) and 21 (e) in an animal treated twice daily with MF. Normalized histograms of mean NADH lifetime of cell regions show a noticeable increase in mean lifetime at days 14 and 21 (f). Scale bar is 50 μm. ps – picoseconds.

obtained from the magnitude of the 2D Fourier transform of the image (31). The orientation index is calculated as

$$N = 1 - \left(\frac{\text{minor Axis}}{\text{major Axis}}\right).$$

This metric takes on values between zero and one where larger values represent more aligned collagen networks. These Fourier transform techniques have been used to accurately quantify both the degree and direction of collagen alignment (32,33). MATLAB (MathWorks, R2014a) was used to calculate the orientation index of local regions of interest (ROI) in each SHG image. To begin, several ROIs of pixel length 40 × 40 were selected from each SHG image for local analysis. The orientation index was calculated as above, and for the entire set of images, the mean local orientation index was calculated to identify the degree of local collagen orientation. Density analysis was performed using a fill fraction metric calculated by counting the number of pixels in each ROI with intensity values greater than the mean intensity of the particular image ROI.

Histological preparation and analysis

After resection of skin samples following imaging, samples were fixed in 10% formalin and paraffin embedded. After embedding, tissue specimens were sectioned (at 5 μm thickness) and stained both for haematoxylin and eosin (H&E) and Masson's trichrome. After staining, a commercial slide scanner (Nanozoomer, Hamamatsu, Hamamatsu, Japan) was used to digitally scan the slides. Images were analysed with the assistance of a board certified veterinary anatomic pathologist utilizing the commercial visualization software provided (OlyVIA 2.6, Olympus, Tokyo, Japan).

Results

Multimodal imaging of *in vivo* skin following steroid treatment

TPEF, FLIM and SHG imaging were performed to visualize the local skin area affected by topical corticosteroid treatment. TPEF images allow visualization of keratinocyte structure (Figure S2a), the SHG images show the collagen structure in the dermis (Figure S2b), and the FLIM images are used to quantify the relative concentration of free and protein-bound NADH (Figure S2c).

Longitudinal tracking of metabolic activity in steroid-treated skin

FLIM was utilized to track the effects of topical steroid application on relative NADH concentrations in order to assess biochemical and molecular intracellular alterations following steroid treatment. Untreated (Figure S3), as well as FP-treated (Fig. 1) and MF-treated (Fig. 2), animals were imaged at each time point. A shift towards longer fluorescence lifetime can be clearly observed in FP-treated animals at day 21 (Fig. 1e) and in MF-treated animals at day 14

(Fig. 2d) and day 21 (Fig. 2e). These shifts in the lifetime can be clearly observed in mean lifetime histograms of the FP (Fig. 1f) and MF (Fig. 2f) groups when compared to untreated animals (Figure S3e). Quantifying the mean lifetime from several skin locations across each group shows a significant increase in fluorescence lifetime in the FP-treated group at day 21 and in the MF-treated group at days 14 and 21 (Fig. 3).

Longitudinal tracking of collagen reorganization in steroid-treated skin

Collagen organization and orientation were visualized using SHG imaging of the dermal layers of the skin. Upon analysis of the acquired images, the organization of dermal collagen was seen to change with both FP and MF treatment. Dense deposits of type I collagen were observed at later time points for FP (Fig. 4b, red ellipse) and MF (Fig. 4c, red ellipse) with strong local alignment when compared to the 'basket weave' appearance seen in untreated animals (Fig. 4a). Quantification of local alignment and density was performed using a localized orientation index based on the two-dimensional spatial Fourier transform of small image blocks as well as a measurement of the fill fraction of pixels with appreciable signal in each image block. These analyses revealed significant increases in the local collagen alignment of the FP-treated group at days 14 and 21 and the MF-treated group at day 21 (Fig. 4d) as well as a significant increase in the fill fraction in the FP-treated group at day 14 and in the MF-treated groups at day 21 (Fig. 4e).

Comparison of results with histology

At various imaging time points, imaged areas of the skin were excised and prepared for histological assessment. Tissues were sectioned and stained with H&E in order to assess the structural alterations of the dermal and epidermal skin layers, and with Masson's trichrome stain to further evaluate the structural properties

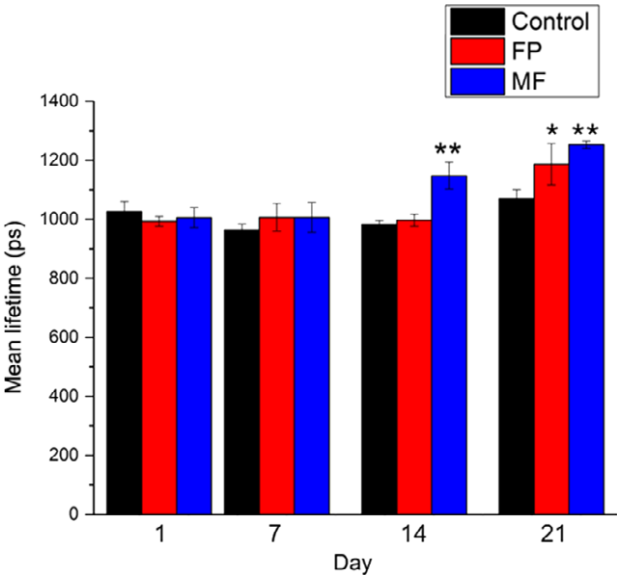

Figure 3. Statistical analysis of mean NADH lifetime measurements. Statistical analysis performed on all animals and imaging locations shows a significant increase in mean lifetime for the FP group at day 21 and for the MF group at days 14 and 21 compared to the control group. Statistical testing performed using Student's t-test * $P < 0.05$; ** $P < 0.01$.

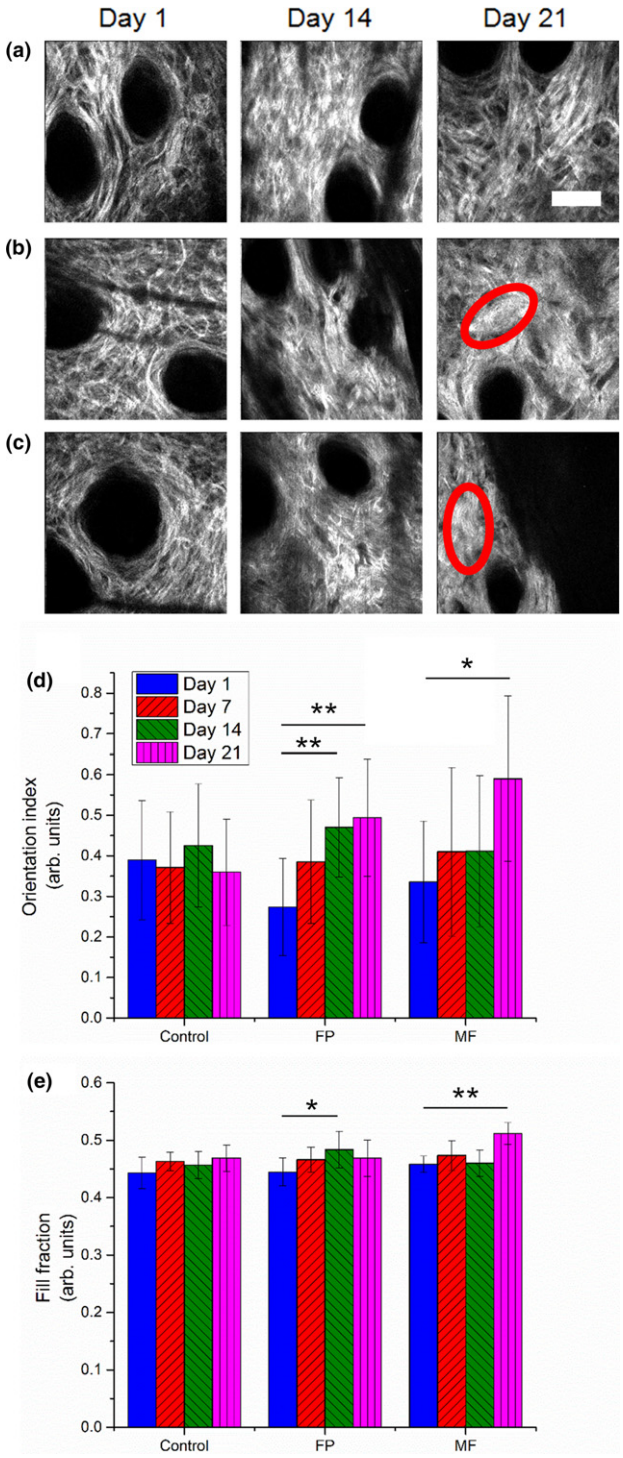

Figure 4. Analysis of dermal collagen reorganization using SHG imaging metrics. SHG images of dermal collagen in untreated (a), FP (b) and MF (c), groups at days 1, 14 and 21 show the reorganization of collagen networks following topical steroid treatment. At 14 and 21 days following treatment, the collagen networks of FP and MF groups are observed to become denser and locally aligned (red ellipses). Further analysis to quantify the local orientation index and SHG fill fraction revealed a significant increase in the local orientation index (d) and fill fraction (e) of FP- and MF-treated groups at day 21 using the Student's t-test. Scale bar is 50 μm. * $P < 0.05$; ** $P < 0.01$.

of the connective tissue in the dermis. Skin thickness changes in hairless mice are typically difficult to assess due to the fact that the normal skin epidermis is only a few cell layers thick and the loss of only a few cell layers can be difficult to quantify (29). Therefore, it is difficult to determine any structural effects of epidermal atrophy from H&E-stained tissue sections for FP (Figure S4b) and MF (Figure S4c) groups compared to the untreated group (Figure S4a). Blue-stained collagen, readily identifiable by Masson's trichrome staining, appeared prominent within the dermis for FP (Figure S4b)- and MF (Figure S4c)-treated groups compared to the untreated group (Figure S4a) at day 21. This prominent appearance in FP- and MF-treated groups likely correlates with the SHG imaging findings.

Discussion

This study presents quantitative findings of the structural and functional alterations of the epidermal and dermal skin microenvironment following treatment with clinically used topical steroids in a dermatological mouse model (29). Results show that structural features identified with traditional histopathological analysis can be identified *in vivo* through non-invasive imaging and tracked longitudinally over time in the same animal. This approach has the potential to significantly reduce the time needed for topical drug efficacy evaluation and may be performed clinically using human subjects. Additionally, functional information related to cell metabolism that was collected and quantified cannot be easily observed with traditional histopathology techniques. For both steroid-treated groups, changes in dermal collagen organization and NADH mean lifetime in epidermal keratinocytes were observed by day 21, suggesting that multimodal optical microscopy may be a useful tool for monitoring and tracking longitudinally the effects of topical steroids.

Epidermal atrophy and thinning due to topical corticosteroid treatment has been characterized previously, and increased rates of cell differentiation without a corresponding increase in cell proliferation rates were identified (10). Thus, keratinocytes were observed to mature at faster rates, differentiating to corneocytes and ultimately being shed off before basal cells are able to divide and replace these lost cells. This can be characterized as a shift from oxidative phosphorylation to glycolysis which will cause an increase in the ratio of protein-bound NADH to free NADH (34). Thus, FLIM measurements of the mean lifetime of keratinocytes not only allow identification of this metabolic shift with subcellular resolution, but also allow quantification of the metabolic changes associated with this shift from oxidative phosphorylation to glycolysis. These FLIM measurements were able to show a large contrast between steroid-treated groups and control groups at later time points that could not be easily identified in histology between the groups. It is also important to note that FLIM measurements of intracellular NADH levels were shown to detect local metabolic alterations at an earlier time point for the MF-treated group than the FP-treated group. As MF is a slightly more potent steroid, this suggests that FLIM also has the potential to identify steroid potency and efficacy *in vivo* before clinically apparent atrophy may be observed. It is also important to note that the conclusions drawn here are based on comparisons to untreated control animals. To fully rule out the effect of the excipients used in each formulation, a deeper study will be necessary with adequate placebo groups in which formulations containing only the excipients are used. Finally, it will be important in future studies to directly confirm the metabolic changes observed in this study. While it remains a challenge to directly confirm the amount of free and protein-bound NADH in cells observed with FLIM measurements, NAD/NADH ratio assays can potentially be used to assess the metabolic profile of cells (35) to confirm the metabolic changes observed. However, this approach would only provide indirect evidence through a general shift in metabolic state.

Dermal reorganization of collagen networks in steroid-treated skin has been described previously using histology and electron microscopy techniques (12). The results from SHG imaging found in this work support the findings of these studies by identifying regions in the upper layers of the dermis in which the local density of collagen deposits was clearly increased. Similar to the observed metabolic changes, evaluation of the effects on the dermal skin layers can be quantified and followed *in vivo* to longitudinally track the effects of topical steroids. However, unlike epidermal atrophy, reorganization of dermal collagen cannot be easily detected or quantified *in vivo* using currently available techniques. SHG imaging together with quantification of the localized orientation index can provide information regarding the structural and organizational changes of collagen.

Using a custom-built integrated, multimodal optical microscope, longitudinal imaging and tracking of increased metabolic processes in rapidly differentiating cells as well as structural remodelling of collagen was observed and quantified non-invasively *in vivo*. This represents an important tool to simultaneously extract structural and functional information at the single cell level in living organisms in order to further understand the longitudinal effects as well as the potential for severe skin atrophy at early time points following topical steroid treatment. As these techniques are label-free and non-invasive, the methods used in this study are widely applicable to many other indications that would affect the metabolic activity in keratinocytes or the structural integrity of the dermal collagen network. In addition to this, these techniques have been used widely for human dermatological imaging (36) and have strong potential for directly evaluating steroid atrophy in human clinical trials. This is useful for understanding and testing the potency of topical steroids in preclinical animal models and may also prove beneficial for diagnostic purposes to more accurately predict the atrophogenic potential in human patients for which topical corticosteroids must be prescribed.

Acknowledgements

We thank Darold Spillman for assistance with logistical and information technology support and Jean-Phillipe Therrien for assistance with the animal model and topical steroid supplies. This research was supported by a sponsored research agreement from GlaxoSmithKline. In this study, A.J.B., Z.A. and Y.Z. performed the research. All authors analysed the data. E.J.C. assisted with animal care and steroid application. Z.A. and S.A.B. designed the experimental study. A.J.B. was supported by the National Science Foundation Graduate Research Fellowship Program (DGE-1 144 245). J.L. was supported by the NIH National Cancer Institute Alliance for Nanotechnology in Cancer programme (Midwest Cancer Nanotechnology Training Center; R25 CA154015A) and a Support for Under-Represented Groups in Engineering (SURGE) Fellowship (University of Illinois at Urbana-Champaign). The authors declare no conflict of interests with regard to this work. Additional information can be found at http://biophotonics.illinois.edu.

Conflict of interest

The authors have declared no conflicting interests.

Supporting Information

Additional supporting data may be found in the supplementary information of this article.

Figure S1. Schematic of integrated multimodal optical microscope. Light from a femtosecond pulsed titanium:sapphire laser is relayed through a pair of scanning mirrors and focused through a high NA objective onto the sample. The resulting TPEF and SHG signals are collected through an optical fiber bundle and detected with a 16 channel PMT spectrometer. Abbreviations: SM – scanning mirror, L – lens, DM – dichroic mirror, OL – objective lens, FB – fiber bundle, PMTS – photomultiplier tube spectrometer.

Figure S2. Multimodal optical imaging of *in vivo* mouse skin. Two-photon excited fluorescence (TPEF) images allow visualization of the keratinocyte cell structure in the epidermis (a). Second harmonic generation (SHG) images show collagen networks in the dermis (b). Fluorescence lifetime imaging microscopy (FLIM) provides metabolic contrast allowing the relative amounts of free and protein-bound NADH to be quantified (c). Acquisition of imaging modalities at different depths can be used to provide a three-dimensional volumetric reconstruction of the skin microenvironment (d). Scale bar is 50 μm.

Figure S3. Longitudinal FLIM imaging of untreated animals. Lifetime imaging of keratinocytes in the epidermis at days 1 (a), 7 (b), 14 (c), and 21 (d) in an untreated control animal. Normalized histograms of mean NADH lifetime of cell regions show a relatively constant level of metabolic activity through 21 days (e). Scale bar is 50 μm. ps – picoseconds.

Figure S4. Histological analysis of steroid treated skin. Images of H&E and Trichrome stained skin samples at day 21 for the control group (a), the FP group (b), and the MF group(c). Masson's Trichrome staining revealed a prominent appearance of blue stained collagen in both FP and MF treated groups (red arrows) which likely correlates with *in vivo* SHG imaging findings. Scale bar is 100 μm.

References

1 Schoepe S, Schäcke H, May E *et al.* Exp Dermatol 2006: **15**: 406–420.
2 Katz H I, Hien N T, Prawer S E *et al.* J Am Acad Dermatol 1987: **16**: 804–811.
3 Kato J S, Fluhr J W, Man M Q *et al.* J Invest Dermatol 2003: **120**: 456–464.
4 Kolbe L, Kligman A M, Schreiner V *et al.* Skin Res Technol 2001: **7**: 73–77.
5 Saarni H, Hopsuhavu V K. Br J Dermatol 1978: **98**: 445–449.
6 Delforno C, Holt P J A, Marks R. Br J Dermatol 1978: **98**: 619–623.
7 Kimura T, Doi K. Toxicol Pathol 1999: **27**: 528–535.
8 Fisher L B, Maibach H I. Arch Dermatol 1971: **103**: 39–44.
9 Zendegui J G, Inman W H, Carpenter G. J Cell Physiol 1988: **136**: 257–265.
10 Laurence E B, Christophers E. J Invest Dermatol 1976: **66**: 222–229.
11 Nuutinen P, Autio P, Hurskainen T *et al.* J Eur Acad Dermatol Venereol 2001: **15**: 361–362.
12 Lehmann P, Zheng P, Lavker R M *et al.* J Invest Dermatol 1983: **81**: 169–176.
13 Schacke H, Docke W D, Asadullah K. Pharmacol Ther 2002: **96**: 23–43.
14 Marks R, Dykes P J, Roberts E. Arch Dermatol Res 1975: **253**: 93–96.
15 Vazquez-Lopez F, Marghoob A A. J Am Acad Dermatol 2004: **51**: 811–813.
16 El Madani H A, Tancrede-Bohin E, Bensussan A *et al.* J Biomed Opt 2012: **17**: 0260091–0260098.
17 Denk W, Strickler J H, Webb W W. Science 1990: **248**: 73–76.
18 Campagnola P J, Millard A C, Terasaki M *et al.* Biophys J 2002: **82**: 493–508.
19 Skala M C, Riching K M, Gendron-Fitzpatrick A *et al.* Proc Natl Acad Sci U S A 2007: **104**: 19494–19499.
20 Lin H J, Herman P, Lakowicz J R. Cytometry A 2003: **52**: 77–89.
21 Agronskaia A V, Tertoolen L, Gerritsen H C. J Biomed Opt 2004: **9**: 1230–1237.
22 Zhong W, Urayama P, Mycek M A. J Phys D Appl Phys 2003: **36**: 1689–1695.
23 Graf B W, Bower A J, Chaney E J *et al.* J Biophotonics 2014: **7**: 96–102.
24 Graf B W, Chaney E J, Marjanovic M *et al.* Technology 2013: **1**: 8–19.
25 Zhao Y, Marjanovic M, Chaney E J *et al.* Biomed Opt Express 2014: **5**: 3699–3716.
26 Zhao Y, Graf B W, Chaney E J *et al.* J Biophotonics 2012: **5**: 437–448.
27 Berth-Jones J, Damstra R J, Golsch S *et al.* BMJ 2003: **326**: 1367.
28 Veien N, Ølholm Larsen P, Thestrup-Pedersen K *et al.* Br J Dermatol 1999: **140**: 882–886.
29 Woodbury R, Kligman A M. Acta Derm Venereol 1992: **72**: 403–406.
30 Balu M, Mazhar A, Hayakawa C K *et al.* Biophys J 2013: **104**: 258–267.
31 Wu S L, Li H, Yang H Q *et al.* J Biomed Opt 2011: **16**: 040502.
32 Osman O S, Selway J L, Harikumar P E *et al.* BMC Bioinformatics 2013: **14**: 260.
33 Sivaguru M, Durgam S, Ambekar R *et al.* Opt Express 2010: **18**: 24983–24993.
34 Stringari C, Edwards R A, Pate K T *et al.* Sci Rep 2012: **2**: 568.
35 Shetty P K, Galeffi F, Turner D A. Neurobiol Dis 2014: **62**: 469–478.
36 König K. J Biophotonics 2008: **1**: 13–23.